# Evaluation of an exact Fourier rebinning algorithm for a large aperture PET scanner

Xuan Liu, Christian Michel, Stefan Vollmar, Klaus Wienhard, Mike Casey, Michel Defrise

## INTRODUCTION

The reconstruction of 3D PET data is a computationally intensive task, especially for dynamic or whole-body studies involving several scans of the same patient. Depending on the available computational hardware, on the type of studies and on the required patient throughput, reconstruction time may still limits the clinical applications of 3D PET. This motivates continuing research for faster reconstruction algorithms for 3D PET data. The fastest methods to date are based on *rebinning methods* [1-7] which factor the 3D field-of-view into a stack of parallel *transaxial slices* and estimate, starting from the measured data, the 2D Radon transform (the sinogram) of the tracer distribution in each of these slices. Rebinning thereby reduces the redundant 3D data to a stack of independent 2D sinograms which can be reconstructed using either 2D filtered-backprojection (FBP) or 2D iterative algorithms such as OSEM.

A practical rebinning method is the *Fourier rebinning algorithm* [FORE 4,5,6,8]. This algorithm is based on the application of the frequency-distance relation to the 2D Fourier transform of each oblique sinogram. The frequency-distance relation is accurate only for large values of the frequency. This is why the accuracy of FORE decreases with increasing values of the angle $\theta$ between the LORs and the transaxial slices. Nevertheless, this algorithm is used routinely by several groups and was shown to be sufficiently accurate for most clinical studies with the current multi-ring PET scanners which have axial apertures not exceeding about $\theta_{max} \approx 15$ degrees. In addition to its approximate character, a second limitation of FORE is that it modifies the statistical properties of the data: contrary to the measured 3D data, the rebinned sinograms are not distributed as independent Poisson variables and hence should not in principle be reconstructed using standard statistical algorithms such as OSEM. In fact, OSEM is a very robust algorithm which has been applied with good results to 2D data rebinned using FORE [8,9,10].

Owing to these two limitations -the approximate character of FORE and its complex effect on data statistics- it is likely that fully 3D iterative algorithms [see e.g. 7] will eventually replace the rebinning algorithms, at least if the available computation power increases more rapidly than the number of LORs acquired by the scanners. Todate, however, fast reconstruction using rebinning algorithms remains attractive for scanners such as the ECAT HHRT [14,15] which acquire data sets which are still too large for a routine application of 3D iterative algorithms. But these scanners are precisely those for which the axial aperture is largest (it exceeds 20 degrees), and for which the approximation in FORE may degrade axial resolution. This was recently demonstrated with phantom studies on the ECAT HRRT scanner [15,16].

These observations suggest to investigate the potential benefit of applying an exact rebinning algorithm, FORE-J [12,13], to the HRRT scanner. This algorithm is exact but can be applied directly to axially truncated data, avoiding the reprojection step required by the reprojection method [3DRP, 17] or by the other exact rebinning algorithm described in the literature, FOREX [18]. The algorithm FORE-J is based on the property that the 3D X-ray transform of a function -the quantity sampled by a 3D PET acquisition- must be solution to the 2nd order partial differential equation (PDE) first studied by F. John. From a practical point of view, FORE-J is easy to implement since it has the same structure as FORE. The only modification is a small correction added to each oblique sinogram prior to rebinning. The calculation of this correction is fast numerically but involves a second derivative of the data with respect to the axial variable $z$, a quantity which is sensitive to noise.

Until now, FORE-J has only been applied to simulated data which did not model the axial undersampling used in practice or the effect of *gaps* in the detectors.
The aim of the present paper is to evaluate the practical usefulness of the algorithm using data from the ECAT HRRT scanner. In particular we
- compare FORE-J with FORE in terms of spatial resolution and clinical image quality,
- investigate the influence of the detector gaps on the use of rebinning algorithms,
- investigate stable yet accurate methods to estimate the second derivative in the FORE-J correction term.

## IMPLEMENTATION OF FORE-J

The HRRT scanner has an axial field-of-view of 25.2 cm and comprises 104 "rings" of detectors. Each "ring" has an octogonal geometry. The list mode data from the HRRT are reorganized into sinograms with 256 radial elements and 288

X.L and M.D. is with the Department of Nuclear Medicine, AZ-VUB, Free University Brussels, Belgium (mdefrise@minf.vub.ac.be).
C.M. and M.C. are with CTI Inc, Knoxville, TN, USA
S.V. and K.W. are with the Max Plank Institute for Neurological Research, Cologne, Germany

angular samples. The radial sinogram sampling interval is 1.22 mm. Because of the junctions between the eight sides of the octogonal detector, the sinograms cannot be measured in eight diagonal bands called "gaps". In the angular variable, each gap covers about 6 samples out of the 288.

To reduce the amount of data to store and process, *axial angular undersampling* (compression) is normally used in the HRRT scanner. In this paper we use the current sinogram set which consists of 2209 sinograms (Span 9, ring difference 67, 325.7 Mbyte) and recovers 88% of the LOR information.

Before applying Fourier based rebinning the gaps in each sinograms are filled with a linear interpolation in the angular direction, using the standard routine in the ECAT software.

The basic equation of the FORE-J algorithm is [12,13]

$$P_{reb}(\omega,k,z_0) = \frac{1}{\delta_{max}} \int_0^{\delta_{max}} d\delta \; (P(\omega,k,z_0 + \frac{k\delta}{\omega},\delta)$$

$$+ \frac{\delta\,(\delta_{max} - \delta)}{\omega} \frac{\partial^3 P(\omega,k,z_0 + \frac{k\delta}{\omega},\delta)}{\partial\omega\partial z^2}) \quad \omega \neq 0$$

In this equation, $P_{reb}(\omega,k,z_0)$ is the 2D Fourier transform of the rebinned sinogram for the transaxial slice $z_0$ and $P(\omega,k,z,\delta)$ is the 2D Fourier transform of a measured oblique sinogram, where $\delta$ is the tangent of the angle $\theta$ between the oblique LORs and the transaxial plane, and $z$ is the axial coordinate of the mid-point of the LORs. The variables $\omega$ and $k$ denote respectively the radial and azimuthal frequencies. The first term in the RHS corresponds to the FORE algorithm, and the second term (second line) is the additive correction in the FORE-J method. The frequencies $\omega$=0 (in practice smaller than some small threshold) are rebinned using a single-slice rebinning approach, using only small values of $\theta$.

For the result presented in this abstract, the second derivative of the sinograms with respect to the axial variable $z$ (the slice index) was estimated using a three point mask (1,-2,1). Alternative methods will be tested.

After rebinning, each sinogram was reconstructed using 2D filtered-backprojection with a ramp filter (rectangular window cut-off at Nyquist's frequency). For the brain scan shown below, the resulting image was smoothed with a 3D gaussian filter with a FWHM of 1.6 pixel.

## RESULTS

### Simulated line source

A line source located in the central transaxial slice (FWHM 2.4 mm) was simulated as a digital 3D image, and 3D data were generated by ray tracing (Joseph's reprojection method with linear interpolation) through this digital image. The axial and transaxial FWHM of the reconstructed line source was estimated as a function of the position along the line.

Figure 1 shows the results obtained with FORE-J, with and without simulated gaps. In the absence of gaps, the transaxial and axial resolutions are almost independent of the radial position, as could be expected since the algorithm is exact and the simulation did not model the position dependence of the detector response. When the gaps are present and are filled by interpolation before rebinning, the axial resolution is degraded by about 0.5 mm. Note that the effect of the gaps on the resolution depends on the radial position.

The comparison with the approximate algorithm FORE (figure 2) illustrates the potential improvement of image quality allowed by the use of an exact rebinning algorithm, at least for a large aperture scanner such as the HRRT.

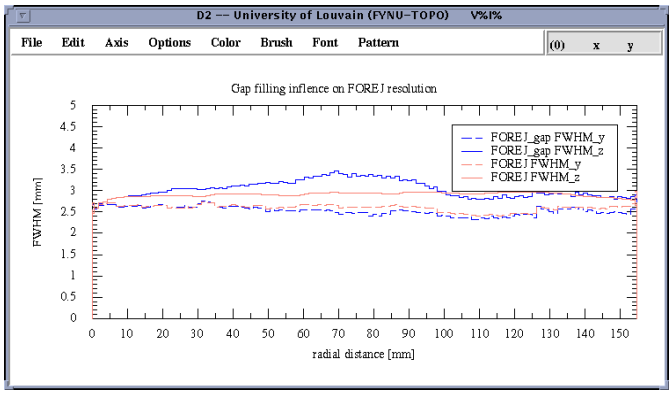


Figure 1. FWHM of the reconstructed simulated line source as function of the radial distance from the axis of the scanner. The axial (full curve) and transaxial (dashed curve) resolutions are shown for the case where the detector gaps are not simulated (red) and for a simulation including the gaps (blue).

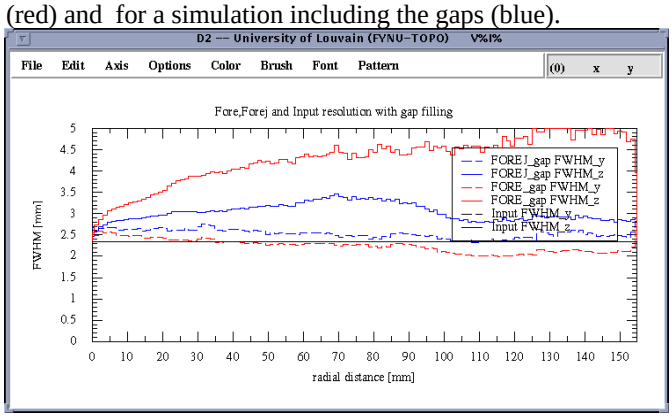


Figure 2. FWHM of the reconstructed simulated line source as function of the radial distance from the axis of the scanner. The axial (full curve) and transaxial (dashed curve) are shown for the FORE (red) and FORE-J algorithms (blue, same data as in figure 1) . The simulation includes the detector gaps. The full horizontal line indicates the FWHM of the simulated line.

Brain scan

An FDG brain scan was reconstructed using both FORE and FORE-J, with a voxel size of 1.22 mm. The total reconstruction time for the two algorithms was respectively 500 s and 717 s. The reconstructions are very similar but FORE-J introduces faint artefacts which appear as horizontal lines in the coronal and sagittal slices, and as rings in the transaxial sections (figures 3). These artefacts are not visible with FORE (not shown) and are tentatively attributed to noise propagation in the calculation of the second derivative. These artefacts are hardly visible on the smoothed images in figure 4 and 5, which would be used in practice. A close inspection of these images, and a comparison with a 3D OSEM reconstruction (8 subsets, 2 iterations, about 4 hours per iteration) reveals several details in the cortical structures which are better reproduced by the FORE-J reconstruction than by FORE. One example shown in figure 6 is the separation between the cortex and the cerebellum (tentorium cerebelli).

## CONCLUSION

Even though the spatial resolution is also limited by the presence of gaps and by the axial undersampling, the exact rebinning algorithm FORE-J significantly improves the axial resolution for the ECAT HRRT scanner. The implementation of FORE-J only requires a minor modification of FORE, which only slightly increases the total reconstruction time. FORE-J appears to better reveal some fine details in the brain scan. However, the preliminary implementation of FORE-J introduces low level artefacts. Alternative methods to discretize the second derivative term in FORE-J will be investigated, and additional tests with phantom ("point" source) and clinical data will be presented at the conference.

## REFERENCES


[1] Daube-Witherspoon M E and Muehllehner G, 1987, Treatment of axial data in three-dimensional PET, J Nucl Med 28, 1717-1724

[2] Erlandsson K, Esser P D, Strand S-E, van Heertum R L, 1994, 3D reconstruction for a multi-ring PET scanner by single-slice rebinning and axial deconvolution, Phys Med Biol 39, 619-629.

[3] Lewitt R M, Muehllehner G and Karp J S, 1994, Three-dimensional reconstruction for PET by multi-slice rebinning and axial image filtering, Phys Med Biol 39, 321-340.

[4] Defrise M, 1995, A factorization method for the 3D X-ray transform, Inverse Problems 11, 983-994.

[5] Tanaka E and Amo Y, 1998, A Fourier rebinning algorithm incorporating spectral transfer efficiency for 3D PET, Phys Med Biol 43, 739-746.

[6] Matej S, Karp J, Lewitt R, Becher A, 1998 Performance of the Fourier rebinning algorithm for PET with large acceptance angles, Phys Med Biol **43** 787-795

[7] Qi J, Leahy R, Hsu C, Fraquar T, Cherry S R, 1997, Fully 3D Bayesian Reconstruction for the ECAT EXACT HR+, Proc IEEE Med Imag Symposium

[8] Liow J-S, Anderson J R, Strother S C 1999, Comparing Reconstruction Algorithms using a Multivariate Analysis, records of the 1999 IEEE Medical Imaging Symposium, Seattle, WA. paper M06-001

[9] Comtat C, Kinahan P E, Defrise M, Michel C and Townsend D W, 1998, Fast reconstruction of 3D PET with accurate statistical modelling, IEEE Trans Nucl Sc NS-45, 1083-1089

[10] Liu X, Comtat C, Michel C, Kinahan P, Defrise M, Townsend D 2001 Comparison of 3D Reconstruction with 3D OSEM and with FORE+OSEM for PET, to be published in IEEE Trans Med Imag

[11] Defrise M, Kinahan P E, Townsend D W, Michel C, Sibomana M and Newport D F, 1997, Exact and approximate rebinning algorithms for 3D PET data, IEEE Trans Med Imag MI-16, 145-158.

[12] Defrise M, Liu X 1999 A fast rebinning algorithm for 3D PET using John's equation, Inverse Problems **15** 1047-1065

[13] Defrise M, Liu X 1999 Fast and exact Fourier rebinning using John's equation, records of the 1999 IEEE Medical Imaging Symposium, Seattle, WA. paper M03-001.

[14] Wienhard K, et al, 1999, Performance Evaluation of a new LSO High Resolution Research Tomograph - HRRT , records of the 1999 IEEE Medical Imaging Symposium, Seattle, WA. paper M04-002.

[15] Wienhard K et al 2000, The ECAT HRRT: Performance and First Clinical Application of a New High Resolution Research Tomograph, records of the 2000 IEEE Medical Imaging Symposium, Lyon, France

[16] Michel C et al 2000, Reconstruction Strategies for the HRRT, records of the 2000 IEEE Medical Imaging Symposium, Lyon, France

[17] Kinahan P E and Rogers J G, 1990, Analytic three-dimensional image reconstruction using all detected events, IEEE Trans Nucl Sci NS-36, 964-968.

[18] Liu X et al 1999, Exact Rebinning Methods for 3D PET, IEEE Trans Med Imag **MI-18** 657-664


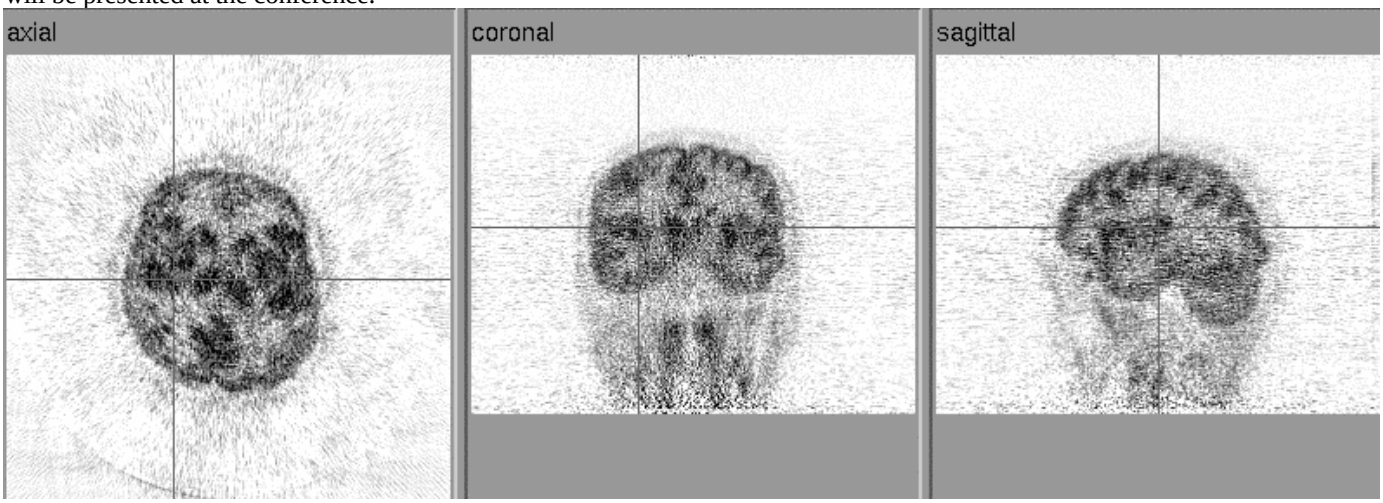


Figure 3. Reconstruction of the brain scan with the exact rebinning algorithm FORE-J, followed by 2D filtered-bacprojection with a rectangular window. Note the ringing artefacts in the transaxial slice.

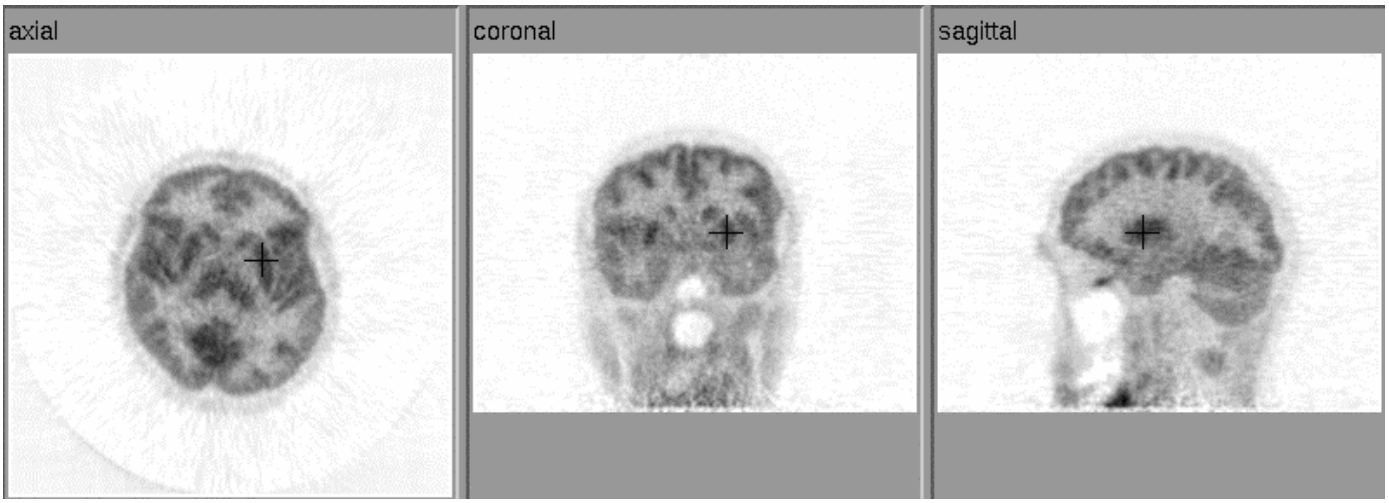


Figure 4. Reconstruction of the brain scan with the exact rebinning algorithm FORE-J, followed by 2D filtered-bacprojection and 3D Gaussian post smoothing (FWHM 1.6 pixel).

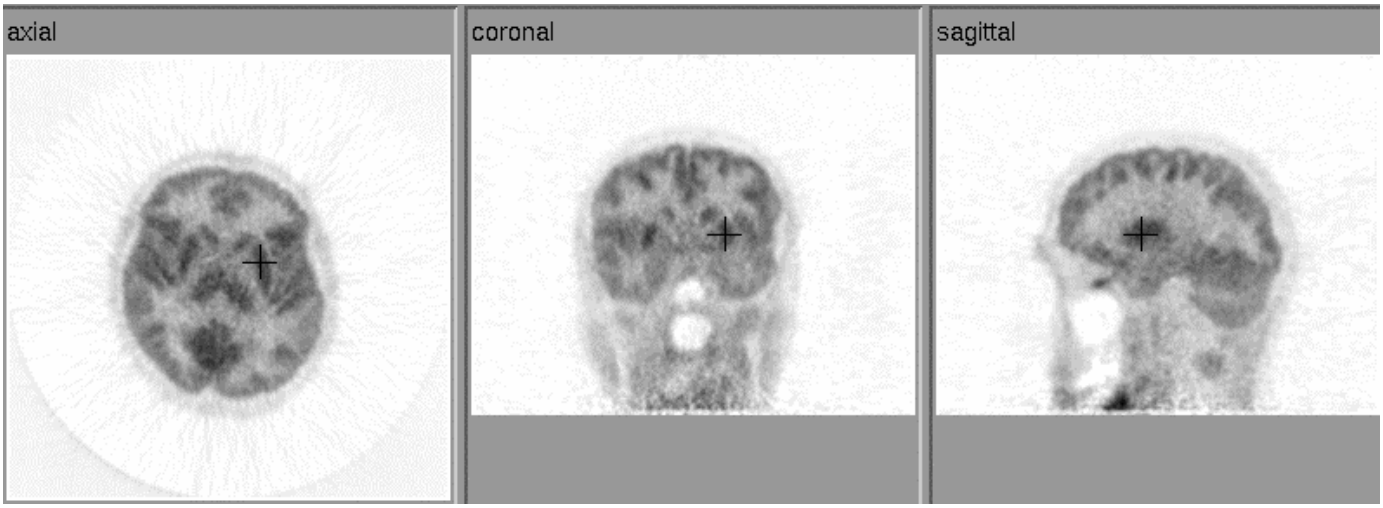


Figure 5. Reconstruction of the brain scan with the approximate rebinning algorithm FORE, followed by 2D filtered-bacprojection and 3D Gaussian post smoothing (FWHM 1.6 pixel).

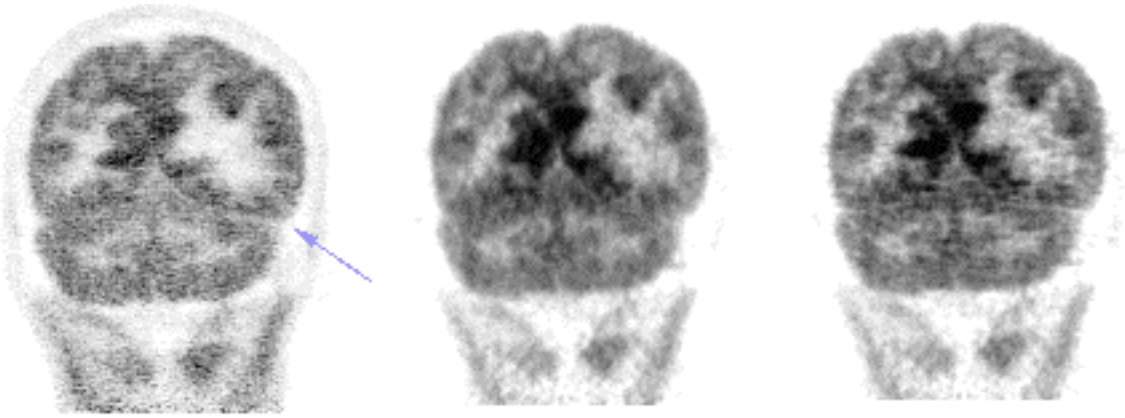

Figure 6. Coronal slice of the brain scan. Left: 3D OSEM with scatter correction, 8 subsets, 2 iterations. Middle: FORE+FBP as in figure 5, Right: FORE-J+FBP as in figure 4 (both without scatter correction). The gray scale is the same for FORE and FORE-J, but not for 3D OSEM. Note the different noise structure and better contrast in the scatter corrected 3D-OSEM image, and the finer detail (arrow) seen in FORE-J than with FORE.